Title

The Nature of Secondary Interactions at Electrophilic Metal Sites of Molecular and Silica-Supported Organolutetium Complexes from Solid-State NMR Spectroscopy.

Journal

Journal of the American Chemical Society, 138(11)

ISSN

0002-7863

Authors

Conley, Matthew P
Lapadula, Giuseppe
Sanders, Kevin
et al.

Publication Date

2016-03-08

DOI

10.1021/jacs.6b00071

Peer reviewed

The Nature of Secondary Interactions at Electrophilic Metal Sites of Molecular and Silica-supported Organolutetium Complexes from Solid-State NMR Spectroscopy

Matthew P. Conley,[1] Giuseppe Lapadula,[1] Kevin Sanders,[2] David Gajan,[2] Lyndon Emsley,[3] Anne Lesage,[2] Iker del Rosal,[4] Laurent Maron,[4] Wayne W. Lukens,[5] Christophe Copéret,[1,*] Richard A. Andersen[6,*]

[1] ETH Zürich, Department of Chemistry, Vladimir Prelog Weg 1-5, CH–8093 Zürich, Switzerland

[2] Université de Lyon, Centre de RMN à Très Hauts Champs, CRNS / ENS-Lyon / UCB Lyon 1, 5 rue de la Doua, 69100 Villeurbanne, France.

[3] Institut des Sciences et Ingénierie Chimiques, Ecole Polytechnique Fédérale de Lausanne (EPFL), CH-1015 Lausanne, Switzerland

[4] Université de Toulouse and CNRS, LPCNO INSA/UPS/CNRS 135, avenue de Rangueil – 31077 Toulouse Cedex 4, France

[5] Chemical Sciences Division, University of California, Lawrence Berkeley National Laboratory, Berkeley, CA 94720 (USA)

[6] Department of Chemistry, University of California, Berkeley, CA 94720, USA

ABSTRACT: The reaction of $Lu[CH(SiMe_3)_2]_3$ with silica partially dehydroxylated at 700 °C gives $[(\equiv SiO)Lu[CH(SiMe_3)_2]_2]$ and $CH_2(SiMe_3)_2$. The surface species is characterized by solid-state NMR and EXAFS spectroscopy, which show that the presence of two carbons and one oxygen in the first coordination sphere corresponding to the surface siloxy and the two residual alkyls, plus additional secondary Lu…C and Lu…O interactions, involving a γ-CH_3 and a siloxane bridge. From X-ray crystallographic analysis, the molecular analogues $Lu[CH(SiMe_3)_2]_{3-x}[O\text{-}2,6\text{-}t\text{Bu-}C_6H_3]_x$ (x = 0, 1 and 2) also have secondary Lu…C interactions. In $Lu[CH(SiMe_3)_2]_3$, the nature of the Lu…C interactions are deduced from solution state ^{1}H NMR spectroscopy in which the –$SiMe_3$ groups are equivalent to –125 °C and inequivalent below that temperature, for which $\Delta G^{\ddagger}_{(Tc = 148\ k)} = 7.1$ kcal mol^{-1}. The proton coupled ^{13}C NMR spectrum of $Lu[CH(SiMe_3)_2]_3$ has $^1J_{CH} = 117 \pm 1$ Hz for both –$SiMe_3$ groups. The solid-state ^{13}C CPMAS NMR spectrum at 20 °C shows three chemically inequivalent resonances in the area ratio of 4:1:1 (12:3:3); the *J*-resolved spectra for each resonance give $^1J_{CH} = 117 \pm 2$ Hz. The ^{29}Si CPMAS NMR spectrum shows two chemically inequivalent resonances with different distinct values of chemical shift anisotropy. Similar observations are obtained for $Lu[CH(SiMe_3)_2]_{3-x}[O\text{-}2,6\text{-}t\text{Bu-}C_6H_3]_x$ (x = 1 and 2). The spectroscopic data points to short Lu…Cγ contact corresponding to a 3c-2e Lu…Cγ-Siβ interactions, which are supported by DFT calculations. Calculated NBO charges show that Cγ carries a negative charge, while Lu, Hγ and Siβ carry positive charges; as the number of O-based ligands increases so does the positive charge at Lu, which in turns shortens the Lu…Cγ distance. The change in NBO charges and the resulting changes in the spectroscopic and crystallographic properties show how ligands and surface-support sites rearrange to accommodate these changes, consistent with Pauling's electroneutrality concept.

Introduction

Weak secondary interactions between a metal and its carbyl ligands are often postulated to play an important role in stabilizing ground states and transition states in catalytic reactions. The interaction implies that electrons in a specific bond in a ligand are in close contact with the electrophilic metal site. These secondary interactions are often encountered in 3-center-2-electron (3c-2e) bond interactions between an empty orbital on the metal with the pair of electrons in a σ-C–H bond and are labeled agostic C-H interaction (Figure 1a).[1] The presence of α-, β-, and/or γ-C-H agostic interactions is often postulated in the transition states for insertion of olefins.[2] For example, the α-CH agostic interaction found in the transition state in metal-catalyzed polymerization of polypropylene is thought to direct the stereoselectivity in the polymer products.[2b, 2c] The insertion of an olefin into an early metal-alkyl bond can generate a γ-CH agostic interaction, which were proposed intermediates in metal-catalyzed olefin polymerization reactions.[1a, 1c] β-C–H Agostic interactions are intermediates in late transition metal olefin polymerization catalysts that undergo chain-walking to form hyper-branched polyolefins.[2d] The agostic interaction is also an important component in stabilizing the *syn*-configuration of Schrock-type alkylidene complexes, essential for the stereoselective production of alkenes in metathesis reactions.[3] This brief outline illustrates that agostic interactions are conceptually important in many metal-catalyzed reactions.[4]

Several structural features are characteristic of ground state β-C–H agostic interactions in d-block transition metals. In general, the C–H bond is elongated, the M…HC is shortened, and the M…CC angles become more acute than ex-

pected for a sp^3-hybridized carbon in the absence of such an interaction.[1c] One of the first structurally characterized complexes containing an agostic interaction was (dmpe)Ti(Et)Cl_3 (dmpe = 1,2-*bis*(dimethylphosphino)ethane), in which the bond distances and angles are summarized in Figures 1a.[5] An α-C-H agostic interactions are also observed in d^0 alkylidene metathesis catalysts documented by acute M-C-H bond angles.[3a, 3d, 3e, 6] In addition to bond distance and angle changes, several spectroscopic observables have been used to support the presence of agostic interactions: the ^{1}H NMR chemical shift in diamagnetic compound of the H-atom involved in an agostic interaction shifts upfield from the free alkane and the $^1J_{CH}$ becomes substantially lower than *ca.* 125 Hz in sp^3 C-H bonds.[1c, 3d, 7] The low coordinate tris-*bis*(trimethylsilyl)methyl lanthanide complexes, Ln[$CH(SiMe_3)_3$]$_3$, with Ln = Y,[8] La,[9] Ce[8] and Sm,[9] contain unusually short distances between the metal and one –$SiMe_3$ group of the pendant alkyl in their X-ray crystal structures. The distortion of a $CH(SiMe_3)_2$ group is also a general pattern observed in the crystal structures of $Cp^*_{3-x}Ln[CH(SiMe_3)_2]_x$, where x = 1 or 2.[10] As noted by Schaverien(Dalton1992) the reasons for these distortions are hindered by the experimental methods used to detect them. Regardless of the reasons, these secondary interactions are a signature of the electrophilicity of the lanthanide in these compoumds.

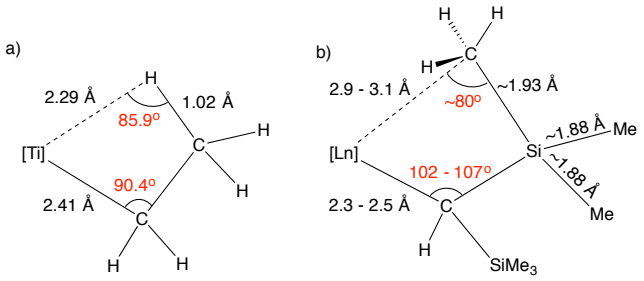

Figure 1. (a) Structural features of the β-CH agostic interaction in (dmpe)Ti(Et)Cl_3; (b) Structural features of the secondary interactions in Ln[$CH(SiMe_3)_2$]$_3$.

In view of our long standing interest in understanding the influence of a surface siloxy group on the reactivity of well-defined supported catalysts,[11] we became interested in using secondary interaction in Ln[$CH(SiMe_3)_3$]$_3$ as a way to evaluate the electrophilicity in silica-supported (≡Si)OLn[$CH(SiMe_3)_2$]$_2$. Here we describe the nature and the strength of metal-hydrocarbyl ligand secondary interactions in organolutetium silica-supported surface species (≡Si)OLu[$CH(SiMe_3)_2$]$_2$ and its corresponding molecular analogues Lu[$CH(SiMe_3)_2$][O–2,6–$tBu_2C_6H_3$], x = 0,1,2. The monomeric, three coordinate molecules have short Lu…Cγ distances in their solid-state crystal structure, the nature of which is defined by solution and solid-state NMR spectroscopies to be 3c-2e Ln…CγSiγ interaction, better described to be a pseudo-bridging methyl between Lu and Si than an agostic Lu…H–Cγ. This experimental deduction is supported by DFT calculations, and in particular NBO charges that depend on the alkyl/alkoxide ratio. The model developed from the molecular compounds is used to rationalize the structure of the supported species (≡Si)OLu[$CH(SiMe_3)_2$]$_2$, obtained by EXAFS spectroscopy. The combination of solution and solid-state spectroscopic studies, supported by the calculation of the NBO charges, provides a detailed understanding of the intramolecular interactions in these molecular and silica-supported organometallic compounds, and documents the role of O-based ligands in tuning the electrophilicity of the lutetium center.

Experimental section.

General considerations. All the experiments were carried under dry, oxygen free argon using Schlenk and glove box techniques. For preparation of surface species, reactions were carried out using high vacuum lines (10^{-5} mbar) and glove box techniques. Pentane was purified using a double MBraun SPS alumina column, degassed before use, and stored over 4Å molecular sieves or by distillation from sodium. Benzene was distilled from purple Na/benzophenone. Deuterated solvents were degassed by three freeze-pump-thaw cycles and distilled from Na/benzophenone by vacuum transfer into flame sealable NMR tubes. Lu[$N(SiMe_3)_2$]$_3$ was synthesized by a modified literature procedure using Lu(OTf)$_3$ and NaN($SiMe_3$)$_2$ in Et_2O; the crude solid was sublimed and the sublimate was crystallized from pentane.[12] Lu[O-2,6-$(Me_3C)_2C_6H_3$]$_3$ was prepared by the reaction of Lu[$N(SiMe_3)_2$]$_3$ and sublimed 2,6-di-t-butylphenol as described in the literature.[13] Silica (Sylapol-948 *ca.* 900 m^2/g) was partially dehydroxylated according a published procedure,[14] and contains 0.35 mmol SiOH g^{-1}. All infrared (IR) spectra were recorded using a Bruker a spectrometer located in an Ar filled glovebox equipped with OPUS software; typically 32 scans were accumulated for each spectrum. Solution ^{1}H, ^{13}C, and ^{29}Si–NMR spectra were obtained using a Bruker DRX 400 spectrometer at room temperature. The ^{1}H, ^{13}C, and ^{29}Si chemical shifts were referenced relative to the residual solvent peaks and reported relative to $SiMe_4$. For the solid–state spectra, a Bruker DRX 700 was used; the MAS frequency was set to 10 kHz for all ^{1}H and ^{13}C spectra, and 5 kHz for ^{29}Si to obtain isotropic chemical shifts. For the CSA analysis, 1.5 kHz spinning was used. Samples were loaded into 4 mm zirconia rotors in the glove box and sealed with PTFE caps. ^{1}H, ^{13}C and ^{29}Si chemical shifts were referenced to external TMS.

EXAFS spectroscopy: Samples were loaded into an aluminum holder equipped with aluminized Mylar windows sealed with an indium gasket in an Ar-filled inert atmosphere glovebox. Assembled holders were sealed in glass jars until just prior to data collection. At the beamline, the jar was opened and the sample was quickly transferred to a helium filled cryostat, which was evacuated then refilled with helium gas three times. Data was obtained at room temperature (the cryostat was only used to provide additional oxygen protection). X-ray absorption data were obtained at beam line 4-1 of Stanford Synchrotron Radiation Lightsource. The x-ray beam was monochromatized using a double crystal monochromator with Si(220) ,ϕ =90° crystals. The second crystal was detuned by 50% to reduce the harmonic content of the beam. Data was obtained in transmission at the lanthanide L_3-edge using N_2-filled ion chambers. Data were deglitched using the EXAFSPAK suite of programs written by Graham George. Data were treated to remove the pre- and post-edge backgrounds and the EXAFS were obtained by subtracting a spline from the absorption data using the software package Athena. EXAFS data were fit using the software package Artemis using theoretical scattering curves generated by Feff7.

EA (Pascher Laboratory).

CRMN Data here

EXAFS.

Computations.

Preparation of Lu[CH(SiMe$_3$)$_2$]$_3$. Lu(O-2,6-tBu$_2$-C$_6$H$_3$)$_3$ (1.20 g, 1.51 mmol) was dissolved in 30 mL of pentane. A solution of Li[CH(SiMe$_3$)$_2$] (0.811 g, 4.89 mmol, 3.2 equiv)[15] was dissolved in a mixture of pentane (90 mL) and toluene (10 mL), and the solution was added to the solution of Lu(O-2,6-Me$_2$-C$_6$H$_3$)$_3$ at 20 °C dropwise over *ca.* 45 min using an addition funnel. A thick-white precipitate formed. The mixture was stirred at room temperature for 16 h. The volatile materials were removed under reduced pressure, resulting in a white solid. Pentane (30 mL) was added by cannula and the insoluble white precipitate was separated by filtration. The clear colorless pentane solution was concentrated to *ca*. 10 mL and cooled to –40 °C. Large clear blocky needles of the product were isolated in two crops by filtration. The needles contain 0.25 equiv of CH$_2$(SiMe$_3$)$_2$ as deduced by the solution ^{1}H NMR spectrum. Yield 0.403 g (41 %). Dissolving the solid in toluene, removing the solvent at high vacuum (10^{-5} mbar), and repeating this treatment seven times yields Lu[CH(SiMe$_3$)$_2$]$_3$*0.39 PhCH$_3$*0.03 CH$_2$(SiMe$_3$)$_2$ according to solution ^{1}H NMR spectroscopy. ^{1}H NMR (C$_7$D$_{14}$, 20 °C): δ 0.36 (18H, s, Lu-CH(Si*Me$_3$*)$_2$, –0.81 (1H, Lu-C*H*(SiMe$_3$)$_2$) and resonances due to toluene and (Me$_3$Si)$_2$CH$_2$; ^{13}C NMR: δ 59.8 (Lu-*C*H(SiMe$_3$)$_2$, $^1J_{CH}$ = 91 Hz), 5.6 (Lu-CH(Si*Me$_3$*)$_2$, $^1J_{CH}$ = 118 Hz). ^{29}Si{^{1}H} NMR: δ –8.7 (s). ^{13}C CPMAS NMR: δ 57.7, 5.4, 4.7, 4.5; ^{29}Si CPMAS NMR: δ –11.75, –5.25. Elemental Analysis: Calcd for C$_{21}$H$_{57}$Si$_6$Lu*(CH$_2$(SiMe$_3$)$_2$)$_{0.25}$: C, 39.41; H, 9.01. Found: C, 39.63; H, 8.95. EIMS (M–15)$^+$ 637 and (M–14)$^+$ 638.

Preparation of Lu[CH(SiMe$_3$)$_2$]$_2$[O-2,6-tBu$_2$-C$_6$H$_3$]. Lu(O-2,6-tBu$_2$-C$_6$H$_3$)$_3$ (0.567 g, 0.72 mmol) was dissolved in 30 mL of pentane. A solution of Li[CH(SiMe$_3$)$_2$] (0.238 g, 1.4 mmol, 2 equiv) dissolved in a mixture of pentane (70 mL) and toluene (5 mL) was added to the solution of Lu(O-2,6-tBu$_2$-C$_6$H$_3$)$_3$ at 20 °C dropwise over *ca.* 45 min using an addition funnel. A thick-white precipitate formed. The mixture was stirred at room temperature for 16 h. The volatile materials were removed under reduced pressure, resulting in a white solid. Pentane (50 mL) was added by cannula, and the insoluble white precipitate was separated by filtration. The clear colorless pentane solution was concentrated to *ca*. 30 mL and placed at –40 °C. Large clear blocks of the product were isolated by filtration. Yield 0.103 g (21 %). ^{1}H NMR (C$_6$D$_6$): δ 7.28 (2H, d, $^3J_{HH}$ = 8 Hz), 6.86 (1H, t, $^3J_{HH}$ = 8 Hz), 1.52 (18H, s), 0.33 (36H, s, Lu-CH(Si*Me$_3$*)$_2$), –0.62 (2H, s, Lu-C*H*(SiMe$_3$)$_2$); ^{13}C NMR: δ 161.2, 137.3, 125.3, 118.3, 51.0 (Lu-*C*H(SiMe$_3$)$_2$, $^1J_{CH}$ = 92 Hz), 34.7, 32.0, 4.8 (Lu-CH(Si*Me$_3$*)$_2$, $^1J_{CH}$ = 117 Hz); ^{29}Si{^{1}H} NMR: δ –8.1 ppm. ^{13}C CPMAS NMR: δ 160.6,136.3, 135.5, 123.2,116.1, 115.5, 55.5, 47.7, 46 .4, 32.9, 32.6, 30.7, 29.3, 4.6, 3.8, 3.0; ^{29}Si CPMAS NMR: δ –3.2, –4.1, –11.9, –12.8. Elemental Analysis: Calcd for C$_{28}$H$_{59}$OSi$_4$Lu: C, 48.14; H, 8.45. Found: C, 48.25; H, 8.51. M.P. 83-85 °C (turned red), EIMS: (M–15)$^+$ 683 and (M–14)$^+$ 684. The compound sublimed at 170-175 °C in diffusion pump vacuum.

Preparation of Lu[CH(SiMe$_3$)$_2$][O-2,6-tBu$_2$-C$_6$H$_3$]$_2$. Lu(O-2,6-tBu$_2$-C$_6$H$_3$)$_3$ (1.22 g, 1.54 mmol) was dissolved in 30 mL of pentane. A solution of Li[CH(SiMe$_3$)$_2$] (0.281 g, 1.70 mmol, 1.1 equiv) was dissolved in a mixture of pentane (90 mL) and toluene (5 mL), and he solution was added to the solution containing Lu(O-2,6-tBu$_2$-C$_6$H$_3$)$_3$ at 20 °C dropwise over *ca.* 45 min using an addition funnel. A thick white precipitate formed. The mixture was stirred at room temperature for 16 h. The volatiles were removed under reduced pressure, resulting in a white solid. Pentane (50 mL) was added by cannula, and the insoluble white precipitate was separated by filtration. The clear colorless pentane solution was concentrated to *ca*. 15 mL and placed at 4 °C. Large clear blocks of the product were isolated by filtration in two crops. Yield 0.546 g (60 %). ^{1}H NMR (C$_6$D$_6$): δ 7.24 (2H, d, $^3J_{HH}$ = 8 Hz), 6.82 (1H, t, $^3J_{HH}$ = 8 Hz), 1.53 (36H, s), 0.36 (18H, s, Lu-CHSi*Me$_3$*), 0.050 (1H, s, Lu-C*H*SiMe$_3$); ^{13}C NMR: δ 160.5, 136.9, 125.4, 118.3, 42.5 (Lu-C*H*SiMe$_3$, $^1J_{CH}$ = 96 Hz), 37.8, 31.9, 4.6 (Lu-CHSi*Me$_3$*, $^1J_{CH}$ = 116 Hz); ^{29}Si{^{1}H} NMR: d –9.0. ^{13}C CPMAS NMR: δ 159.5, 158.2, 135.4, 134.7, 134.2, 125.3, 123.0, 122.8, 121.4, 116.6, 116.3, 42.8, 32.9, 32.6, 30.9, 30.2, 29.6, 29.3, 2.8; ^{29}Si CPMAS NMR: δ –4.6, –13.4. Elemental Analysis: Calcd for C$_{35}$H$_{61}$O$_2$Si$_2$Lu: C, 56.43; H, 8.25. Found: C, 56.15; H, 8.46.

Grafting Lu(CH(SiMe$_3$)$_2$)$_3$ on [SiO$_{2-700}$]. Sylapol-948 dehydroxylated at 700 °C (0.106 g, 0.10 mmol SiOH) was contacted with a C$_6$H$_6$ solution (2 mL) containing Lu(CH(SiMe$_3$)$_2$)$_3$ (0.075 g, 0.11 mmol) for 3.5 h. The solution was filtered, and the solid was washed with benzene (3 x 2 mL), then with pentane (5 mL), and the solid was dried on a high vacuum line for 1h. The combined benzene filtrate contained 0.10 mmol (Me$_3$Si)$_2$CH$_2$ by ^{1}H NMR relative to Cp$_2$Fe as an internal standard. ^{1}H MAS NMR: δ 0.1 (Lu-CH*(SiMe$_3$)*$_2$), -0.8 (Lu-C*H*(SiMe$_3$)$_2$); ^{13}C CPMAS NMR: δ 50 and 3 ppm; ^{29}Si CPMAS NMR: -8 and -6 ppm. Elemental Analysis: 6.07 % Lu, 5.94 % C

Results

Synthesis of Lu[CH(SiMe$_3$)$_2$]$_{3-x}$[O-2,6-tBu$_2$-C$_6$H$_3$]$_x$ (x = 0,1,2)

Addition of Li[CH(SiMe$_3$)$_2$] in a mixture of pentane/toluene to the aryloxide Lu[O-2,6-*t*Bu$_2$-C$_6$H$_3$]$_3$ forms the lutetium alkyl compounds and Li[O-2,6-*t*Bu$_2$-C$_6$H$_3$] as illustrated in Scheme 1. The extent of alkylation depends on the stoichiometry of the reactants; three equivalents afford Lu[CH(SiMe$_3$)$_2$]$_3$ and one or two equivalents of Li[CH(SiMe$_3$)$_2$] afford Lu[CH(SiMe$_3$)$_2$][O-2,6-*t*Bu$_2$-C$_6$H$_3$]$_2$ or Lu[CH(SiMe$_3$)$_2$]$_2$[O-2,6-*t*Bu$_2$-C$_6$H$_3$], respectively. All three alkyl derivatives are isolated by crystallization from pentane as clear colorless crystals. The specific product formed is determined by the reaction stoichiometry, which implies that the individual compounds are stable to ligand redistribution reactions in hydrocarbon solution at 20 °C. Solutions of Lu[CH(SiMe$_3$)$_2$]$_2$[O-2,6-*t*Bu$_2$-C$_6$H$_3$] or Lu[CH(SiMe$_3$)$_2$][O-2,6-*t*Bu$_2$-C$_6$H$_3$]$_2$ in C$_6$D$_6$ at 20 °C are stable for over one month, indicating that this implication is correct.

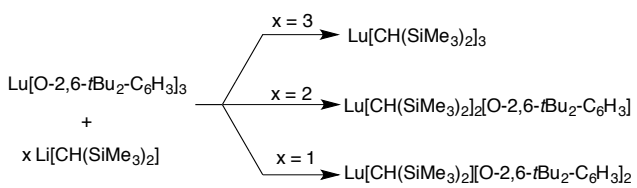

Scheme 1. Synthesis of Lu[CH(SiMe$_3$)$_2$]$_{3-x}$[O-2,6-tBu$_2$-C$_6$H$_3$]$_x$ (x = 0,1,2)

Reaction of $Lu[CH(SiMe_3)_2]_3$ with Partially Dehydroxylated Silica

Contacting silica partially dehydroxylated at 700 °C (0.35 mmol $OH.g^{-1}$) with benzene solutions of $Lu[CH(SiMe_3)_2]_3$ yields 1.0 equiv of $CH_2(SiMe_3)_2$ per surface silanol. The infrared spectrum of the resulting material, $(\equiv SiO)Lu[CH(SiMe_3)_2]_2$ (Scheme 2), lacks the ν_{OH} vibrations characteristic of free surface silanols, indicating that $Lu[CH(SiMe_3)_2]_3$ grafts quantitatively on the silica surface (see Supporting Information). This material contains 6.07 % Lu, corresponding to 0.347 mmol g^{-1}, with 14 ± 1 C/Lu from elemental analysis that supports the stoichiometry of Scheme 2.

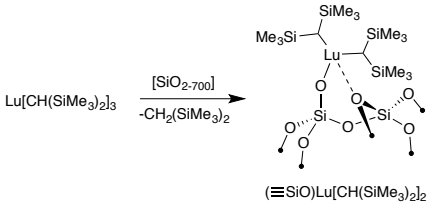

Scheme 2. Reaction of $Lu[CH(SiMe_3)_2]_3$ and $[SiO_{2\text{-}700}]$ to form $(\equiv SiO)Lu[CH(SiMe_3)_2]_2$

The solid state ^1H Magic Angle Spinning (MAS) NMR spectrum of $(\equiv SiO)Lu[CH(SiMe_3)_2]_2$ contains two signals at –0.6 ppm and 0.3 ppm, assigned to the α-CH and the methyl groups of $–SiMe_3$, respectively. These chemical shifts are similar to the values obtained for $Lu[CH(SiMe_3)_2]_2[O\text{-}2,6\text{-}tBu_2\text{-}C_6H_3]$ in C_6D_6 solution of –0.62 and 0.33 ppm, respectively. The ^{13}C Cross Polarization Magic Angle Spinning (CPMAS) spectrum of $(\equiv SiO)Lu[CH(SiMe_3)_2]_2$ with short contact time (600 ms) contains two resonances at 50 and 3 ppm assigned to the Lu-C*H* and –Si*Me*$_3$ groups, respectively, which may be compared to the resonances at 51.0 and 4.8 ppm in $Lu[CH(SiMe_3)_2]_2[O\text{-}2,6\text{-}tBu_2\text{-}C_6H_3]$ in C_6D_6. The ^{29}Si CPMAS NMR spectrum contains two signals at –8 and –6 ppm, indicating to the presence of two inequivalent silicons in $(\equiv SiO)Lu[CH(SiMe_3)_2]_2$; a solution of $Lu[CH(SiMe_3)_2]_2[O\text{-}2,6\text{-}tBu_2\text{-}C_6H_3]$ has a single ^{29}Si resonance at –8.1 ppm. The spectra of $(\equiv SiO)Lu[CH(SiMe_3)_2]_2$ are available in the Supporting Information.

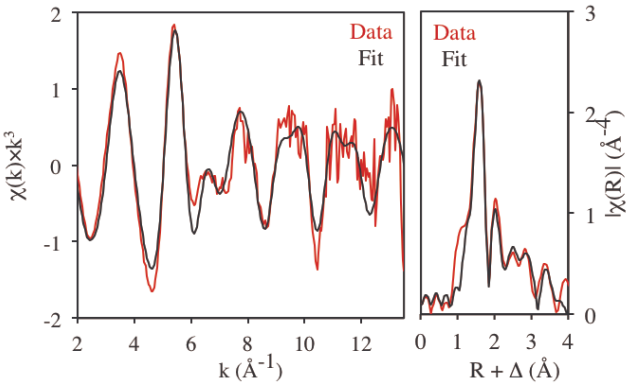

Figure 2. Lu L_3-edge EXAFS spectrum of $(\equiv SiO)Lu[CH(SiMe_3)_2]_2$.

Table 1. EXAFS parameters for $(\equiv SiO)Lu[CH(SiMe_3)_2]_2$

Element	# of atoms[a]	Distance (Å)	s^2 (Å^2)	p
O	1	2.038(7)	0.0040(6)	<0.001
C	2	2.32(1)	0.011(2)	<0.001
C	1	2.80(2)	0.006(2)	0.003
O	1	3.23(2)	0.004(1)	0.002
C	1	3.87(2)	0.002(2)	0.061

a) S_0^2=1 (fixed), DE_0 = 7(1) eV

The Extended X-ray Absorption Fine Structure (EXAFS) fit for the silica-supported species is shown in Figure 2, and the results of the fitting are summarized in Table 1. The short Lu-O distance (2.04 Å) is assigned to a surface siloxy group and is close to Lu-O bond distances reported for alkoxide and aryloxide complexes (2.0 - 2.1 Å)[16] and to the average Lu–O distance in $Lu[CH(SiMe_3)_2]_2[O\text{-}2,6\text{-}tBu_2\text{-}C_6H_3]$ of 2.032 ± 0.006 Å for the two independent molecules in the unit cell, see below. Two carbon atom scatters at 2.32 Å are assigned to the Lu-*C*H$(SiMe_3)_2$ carbons that are near the average value of the Lu–C bond distance obtained in the solid-state structure of $Lu[CH(SiMe_3)_2]_2[O\text{-}2,6\text{-}tBu_2\text{-}C_6H_3]$ of 2.32 ± 0.02 Å, see below. The next scattering shell contains long range Lu–O and Lu–C scatters at 3.23 Å and 3.87 Å, respectively. Interestingly, one carbon atom at 2.80 Å must be included in the fit, and is attributed to a secondary Lu…Cγ interaction. In the crystal structure of $Lu[CH(SiMe_3)_2]_2[O\text{-}2,6\text{-}tBu_2\text{-}C_6H_3]$ shown in Figure 3a two Lu…Cγ distances of 2.66 ± 0.03 and 2.70 ± 0.02 Å are observed.

Solid-state Structures of $Lu[CH(SiMe_3)_2]_{3\text{-}x}[O\text{-}2,6\text{-}tBu_2\text{-}C_6H_3]_x$ (x = 0,1,2)

Single crystals of $Lu[CH(SiMe_3)_2]_3$, $Lu[CH(SiMe_3)_2]_2[O\text{-}2,6\text{-}tBu_2\text{-}C_6H_3]$, and $Lu[CH(SiMe_3)_2][O\text{-}2,6\text{-}tBu_2\text{-}C_6H_3]_2$ were grown from concentrated pentane solutions, and their solid-state structures are shown in Figures 3 and 4, respectively. Selected bond distances and angles are given in Table 2, and crystal data are available in the Supporting Information.

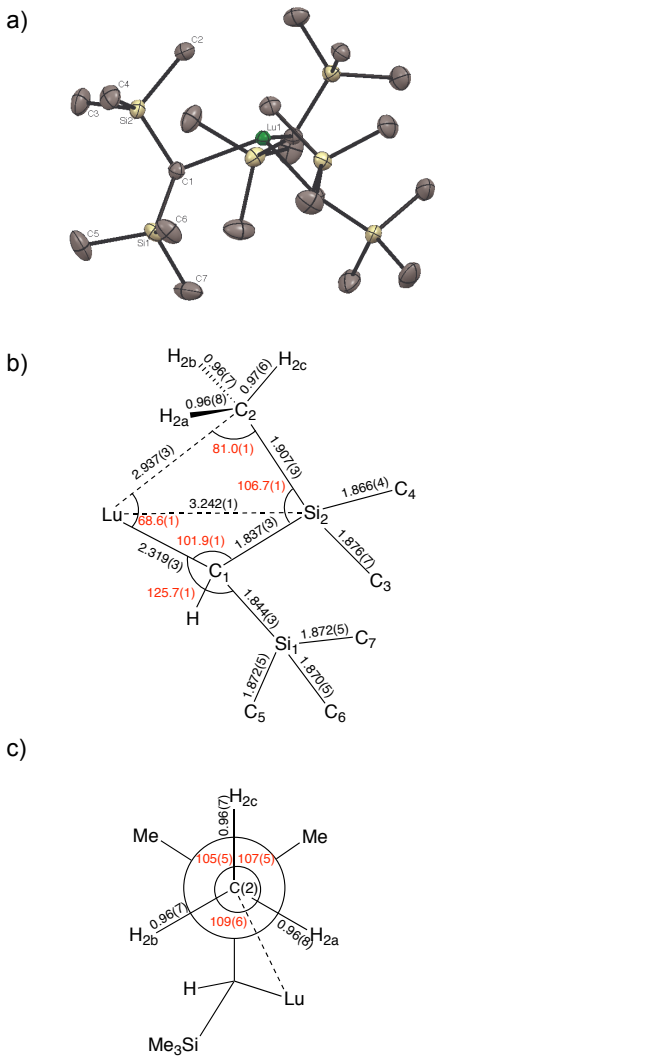

Figure 3. a) ORTEP of $Lu[CH(SiMe_3)_2]_3$ with 50 % probability ellipsoids. The heavy atoms are refined anisotropically and the hydrogen atoms are located and refined isotropically. For clarity the hydrogen atoms and the 0.3 equiv of disordered $CH_2(SiMe_3)_2$ are omitted. Selected distances and angles are shown in Table 2; b) sketch of relevant bond lengths (Å in black) and angles (°, red) in $Lu[CH(SiMe_3)_2]_3$; c) Neumann projection down the C(2)–Si(2) bond with bond lengths and angles (in red) obtained from the crystal structure of $Lu[CH(SiMe_3)_2]_3$.

The ORTEP of $Lu[CH(SiMe_3)_2]_3$ is shown in Figure 3a and summarized graphically in Figure 3b. As found in other $Ln[CH(SiMe_3)_2]_2$ complexes (La, Ce and Sm),[8-9] $Lu[CH(SiMe_3)_2]_3$ crystallizes in the $P31_C$ space group. The crystal contains 0.3 equiv of disordered $CH_2(SiMe_3)_2$ in the unit cell. $Lu[CH(SiMe_3)_2]_3$ adopts a pyramidal geometry with lutetium out of the plane defined by the three carbon atoms by 0.89 Å. The Lu–C(1) distance is 2.319(3) Å, similar to those found in other $Ln[CH(SiMe_3)_2]_3$ complexes. The molecule has C_3 symmetry since the $-SiMe_3$ groups are oriented like the blades of a propeller.[8-9] The Lu…C(2) distance is 2.937(4) Å, and the Lu…Si(2) distance is 3.242(1) Å. The asymmetry in the Lu…C(2) and Lu…Siβ distances are associated with the Lu…C(1) Si(2) and Lu…C(1)Si(1) angles of 101.9(1) and 127.7(1) °, respectively. The Si–C bond lengths are often used as indicators for the presence or absence of secondary Siγ–Cγ interaction in $Ln[CH(SiMe_3)_2]_3$ compounds. In $Lu[CH(SiMe_3)_2]_3$ the Si(2)–C(2) distance is 1.907(3) Å, significantly lengthened relative to the other five Si(2)–C(3,4) and Si(1)-C(5,6,7) distances that average to 1.871 ± 0.005 Å.

The observation of asymmetry in bond lengths and angles in the lutetium alkyl-related compounds is generally ascribed as an agostic M…H–Cγ or a M…Cγ–Siβ interaction.[17] A distinction between these two descriptions can be made by analyzing the orientation of hydrogen atoms on the C(2) methyl group, that is, whether they are pointed towards or away from the metal in the crystal structure, and the $^1J_{CH}$ values in the ^{13}C NMR spectrum. As shown in Figure 3c, the orientation of the C(2)-H(2a,b,c) bonds in $Lu[CH(SiMe_3)_2]_3$, which are located and refined isotropically, are oriented away from Lu with H–Cγ–H angles close to tetrahedral values. The Lu–C(1)–C(2)–H(2c) torsion angle is 176(7)°, while the Lu–C(1)–C(2)–H(2a) and Lu–C(1)–C(2)–H(2b) torsion angles are 66(4)° and 43(4)°, respectively. These torsion angles are inconsistent with that expected for an agostic M…H–Cγ interaction, though consistent with a 3c–2e M…Cγ–Siβ interaction as originally suggested by Morokuma.[18] A similar set of torsion angles is found in $Yb(dmpe)[N(SiMe_3)_2]_2$,[19] $Ln[CH(SiMe_3)_3]_3$ (Ln = Y,[8] La,[9] Ce[8] and Sm[9]) and in the Neutron diffraction structure of $Cp^*La[CH(SiMe_3)_2]_2$[20] and interpreted similarly. This contention is supported by solution, and more importantly, solid-state NMR spectra of $Lu[CH(SiMe_3)_2]_3$ described in the following section.

The ORTEP's for $Lu[CH(SiMe_3)_2]_2[O\text{-}2,6\text{-}t\text{Bu}_2\text{-}C_6H_3]$ and $Lu[CH(SiMe_3)_2][O\text{-}2,6\text{-}t\text{Bu}_2\text{-}C_6H_3]_2$ are shown in Figures 4a and 4b, respectively. Both of these molecules crystallize with two independent molecules in their unit cells, only one of which is shown in the Figure; the other ones can be found in the SI (Figure SX). One of the Lu–$CH(SiMe_3)_2$ fragments in one independent molecule of $Lu[CH(SiMe_3)_2]_2[O\text{-}2,6\text{-}t\text{Bu}_2\text{-}C_6H_3]$ is disordered and was refined in two positions. The crystal data and all of the bond lengths and angles for the independent molecules are available in the SI, selected bond distances and angles for the independent molecules are listed in Table 2.

The geometry of $Lu[CH(SiMe_3)_2]_2[O\text{-}2,6\text{-}t\text{Bu}_2\text{-}C_6H_3]$ and $Lu[CH(SiMe_3)_2][O\text{-}2,6\text{-}t\text{Bu}_2\text{-}C_6H_3]_2$ are similar as the lutetium atom lies in the plane defined by the carbon and oxygen atoms, which is in contrast to that in $Lu[CH(SiMe_3)_2]_3$ and $Lu[O\text{-}2,6\text{-}t\text{Bu}_2\text{-}C_6H_3]_3$.(ref) As the number of $[O\text{-}2,6\text{-}t\text{Bu}\text{-}C_6H_3]$ groups in $Lu[CH(SiMe_3)_2]_{3\text{-}x}[O\text{-}2,6\text{-}t\text{Bu}_2\text{-}C_6H_3]_x$ increases from one, to two, to three the Lu–O distance slightly decreases from 2.032 ± 0.006 Å to 2.014 ± 0.004 Å to 2.013 ± 0.002 Å, respectively. The Lu–Cα distance does not change as the number of $[CH(SiMe_3)_2]_3$ ligand decreases from three to two to one; the values are 2.319(3) Å, 2.32 ± 0.02 Å, and 2.324 ± 0.007 Å, respectively. However, the Lu…Cγ distances shorten in the order of 2.937(3) Å to 2.69 ± 0.02 Å to 2.598 ± 0.008 Å as do the Lu…Siβ distances, 3.242(1) to 3.10 ± 0.01 Å to 3.048 ± 0.002 Å, respectively. These changes presumably reflect the electronegativity increase of oxygen relative to carbon, a conjecture that is corroborated by the NBO charges that are presented in the computational section.

Table 2. Selected of bond lengths (Å) and angles (°) for $Lu[CH(SiMe_3)_2]_3$, $Lu[CH(SiMe_3)_2]_2[O\text{-}2,6\text{-}t\text{Bu}_2\text{-}C_6H_3]$, and $Lu[CH(SiMe_3)_2][O\text{-}2,6\text{-}t\text{Bu}_2\text{-}C_6H_3]_2$

	M–Cα	M…Cγ	M…Siβ[a]	Siβ–Cγ	M–Cα–Siβ		Cα–Siβ–Cγ
$Lu[CH(SiMe_3)_2]_3$	2.319(3)	2.937(3)	3.242(1)	1.908(2)[b] 1.871(4)[c]	101.9(1) 125.7(4)		106.7(1)
$Lu[CH(SiMe_3)_2]_2[O\text{-}2,6\text{-}t\text{Bu}_2\text{-}C_6H_3]$							
Molecule 1	2.29(6)	2.67(1)	3.095(4)	1.89(1)[b]	96.8(7)	96.3(5)	106.0(6)
	2.32(1)	2.74(1)	3.111(4)	1.86(2)[c]	139.3(8)	133.0(6)	
Molecule 2	2.31(2)	2.71(4)	3.13(3)	1.87(2)[c]	89(1) 99(1)	94.6(6)	103(1)
	2.33(2)	2.64(5)	3.07(1)	2.01(3)[b]	138(1)	135.4(7)	101(1)
	2.35(1)	2.69(1)	3.107(4)	1.86(3)[c]	129(1)		
$Lu[CH(SiMe_3)_2][O\text{-}2,6\text{-}t\text{Bu}_2\text{-}C_6H_3]_2$							
Molecule 1	2.317(7)	2.595(7)	3.042(7)	1.917(7)[b]	93.0(3)		107.8(3)
				1.860(8)[c]	123.1(3)		
Molecule 2	2.331(7)	2.601(8)	3.054(2)	1.917(7)[b]	93.3(9)		106.9(3)
				1.867(7)[c]	123.5(3)		

[a] Distance from Lu to the proximal Siβ. [b] The Cα atoms are disordered in both molecules. [c] Siβ–Cγ proximal to the lanthanide atom. [d] average of all Siβ–CγCγ

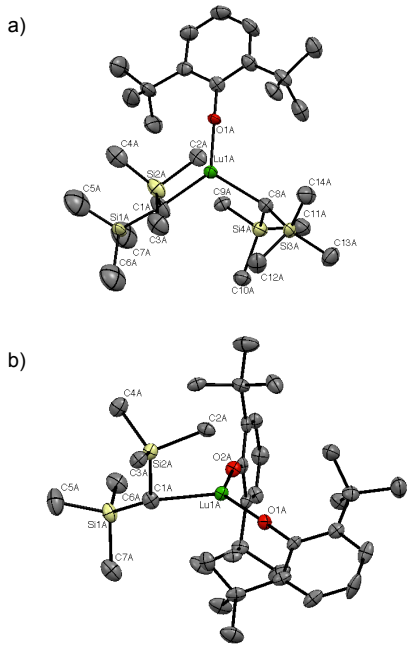

Figure 4. a) ORTEP of a molecule in the unit cell of $Lu[CH(SiMe_3)_2]_2[O\text{-}2,6\text{-}t\text{Bu}_2\text{-}C_6H_3]$, the thermal ellipsoids are at 50 % probability. For clarity the hydrogen atoms are omitted. Non-hydrogen atoms are refined anisotropically and the hydrogen atoms are placed in the calculated positions and not refined. The carbon atoms 1A and 8A are disordered; b) ORTEP of one of the molecules in the unit cell of $Lu[CH(SiMe_3)_2][O\text{-}2,6\text{-}t\text{Bu}_2\text{-}C_6H_3]_2$ at 50 % probability. For clarity the hydrogen atoms are omitted. Non-hydrogen atoms are refined anisotropically and the hydrogen atoms are placed in the calculated positions and not refined. Selected distances and angles are shown in Table 2.

Solution NMR Properties of $Lu[CH(SiMe_3)_2]_{3-x}[O\text{-}2,6\text{-}t\text{Bu}_2\text{-}C_6H_3]_x$ (x = 0,1,2)

The presence of short Lu…Cγ distances in $Lu[CH(SiMe_3)_2]_3$ implies that the chemically inequivalent $-SiMe_3$ groups should appear in a 3:3:3:9 ratio in the ^{1}H NMR spectrum.[21] The ^{1}H NMR spectrum of $Lu[CH(SiMe_3)_2]_3$ at 20 °C in methylcyclohexane-d_{14} contains a single sharp resonance for the $-SiMe_3$ groups at 0.36 ppm as does the ^{29}Si NMR spectrum at –8.6 ppm. The ^{13}C NMR spectrum at 20 °C contains two resonances at 59.8 ppm ($^1J_{CH}$ = 91 Hz) and at 5.6 ppm ($^1J_{CH}$ = 118 Hz) for the Lu-*C*α and the –Si*Me*$_3$ groups, respectively. These observations indicate that the $-SiMe_3$ groups are undergoing fast site exchange at this temperature. Cooling the sample in methylcyclohexane-d_{14} results in minimal line broadening until –100 °C. At –120 °C the resonance broadens but does not decoalesce, and the slow exchange limit is not reached in this solvent. However, further cooling a solution of $Lu[CH(SiMe_3)_2]_3$ in 2-methylbutane-d_{12} results in decoalesence at *ca.* –125 °C as two equal area resonances emerge, $\Delta G^{\ddagger}_{(Tc = 148K)}$ = 7.1 kcal mol^{-1} (Figure SX). At –140 °C the downfield resonance is broader than that of the upfield resonance indicating that rotation about the Cα–Siβ bonds are still rapid on the ^{1}H NMR timescale but the rates are not equal. This result suggests that the downfield resonance is involved in the Lu…Cγ–Siβ interaction observed in the crystal structure. The variable temperature ^{13}C{^{1}H} NMR spectra are qualitatively similar to the ^{1}H NMR spectra since the single $-SiMe_3$ resonance broadens by –125 °C and two distinct resonances emerge by –140 °C, the upfield resonance being broader than the downfield one, Figure S3b. The $^1J_{CH}$ coupling constants are 117 ± 1 Hz for both resonances in the chemically inequivalent $-SiMe_3$ groups at –140 °C.

In C_6D_6 solution the ^{1}H NMR spectrum of $Lu[CH(SiMe_3)_2]_2[O\text{-}2,6\text{-}t\text{Bu}_2\text{-}C_6H_3]$ contains a sharp signal at 0.33 ppm for the Lu–CH(Si*Me*$_3$)$_2$ groups, and the ^{13}C NMR spectrum has a resonance at 5.6 ppm due to these carbons. The $^1J_{CH}$ of the Lu–CH(Si*Me*$_3$)$_2$ group is 118 Hz, as in $Lu[CH(SiMe_3)_2]_3$. The lower solubility of $Lu[CH(SiMe_3)_2]_2[O\text{-}2,6\text{-}t\text{Bu}_2\text{-}C_6H_3]$ in 2-methylbutane-d_{12} prohibits a quantitative study at very low temperatures, but qualitatively, $Lu[CH(SiMe_3)_2]_2[O\text{-}2,6\text{-}t\text{Bu}_2\text{-}C_6H_3]$ has a similar profile as $Lu[CH(SiMe_3)_2]_3$. At –130 °C, the $-SiMe_3$ groups appear as three broad signals at 0.38, 0.28, and 0.041 ppm. These resonances coalesce at –120 °C indicating a low barrier for rotation of the Lu–Cα bond. Cooling the sample to –137 °C results in further

line broadening, but the slow exchange limit is not reached. The combination of reduced solubility in 2-methylbutane-d_{12} and the intermediate exchange rates encountered in the variable temperature ^{1}H NMR study inhibits a quantitative analysis of the ^{13}C NMR spectra at low temperatures.

The NMR spectra of Lu[CH(SiMe$_3$)$_2$][O-2,6-*t*Bu$_2$-C$_6$H$_3$]$_2$ are similar to those of Lu[CH(SiMe$_3$)$_2$]$_2$[O-2,6-*t*Bu$_2$-C$_6$H$_3$] and Lu[CH(SiMe$_3$)$_3$]$_3$. The ^{1}H NMR spectrum of Lu[CH(SiMe$_3$)$_2$][O-2,6-*t*Bu$_2$-C$_6$H$_3$]$_2$ in C$_6$D$_6$ at 20 °C contains sharp signals at 0.33 ppm for Lu–C*H*(SiMe$_3$)$_2$ and 0.050 ppm for Lu–CH(Si*Me$_3$*)$_2$, respectively, indicating fast site exchange between the two –SiMe$_3$ groups. The ^{13}C NMR spectrum contains a sharp signal for the methyl group at 4.8 ppm with $^1J_{CH}$ of 117 Hz. The monoalkyl is insoluble in 2-methylbutane-d_{12}, but the ^{1}H NMR spectrum in toluene-d_8 at –90 °C contains broad signals for the –SiMe$_3$ and –*t*Bu groups, indicating that the slow exchange limit is not reached by this temperature (Figure SX).

Solid-State NMR of Lu[CH(SiMe$_3$)$_2$]$_{3-x}$[O-2,6-tBu$_2$-C$_6$H$_3$]$_x$ (x = 0,1,2)

Although the site exchange between the two SiMe$_3$ groups is slow below –125 °C in the solution ^{1}H spectrum of Lu[CH(SiMe$_3$)$_2$]$_3$, rotation about the Siβ–Cγ bond is still rapid at –140 °C. Although the solid-state crystal structure shows one short Lu…Cγ contact distance, this stereochemical feature is not resolved at –140 °C, and the nature of this interaction is not defined in solution. Solid-state NMR spectroscopy provides a definitive answer. The ^{29}Si Cross Polarization Magic Angle Spinning (CPMAS) spectrum of Lu[CH(SiMe$_3$)$_2$]$_3$ obtained at 5 kHz spinning speed contains two sharp signals at –5.3 and –11.7 ppm, indicating that the silicon atoms are inequivalent and that the rate of site exchange is slow in the solid state. The ^{13}C CPMAS spectrum of Lu[CH(SiMe$_3$)$_2$]$_3$ at 10 kHz, shown in Figure 5a, contains signals from Lu–*C*H(SiMe$_3$)$_2$ at 57.7 ppm and for the Lu–CH(Si*Me$_3$*)$_2$ groups at 4.5, 4.7, and 5.4 ppm in a 1:1:4 area ratio at 20 °C. Assuming that the chemical shift of one SiMe is degenerate with that of the three equivalent SiMe$_3$ groups, the 1:1:4 pattern may be rationalize from the crystal structure, since the proximal –SiMe$_3$ group has C_1 local symmetry. NMR relaxation measurements show that the signals at 4.5 and 4.7 ppm have shorter T_2' values (32 and 31 ms, respectively) than the signal at 5.4 ppm (T_2' = 85 ms), indicating a more rigid environment is experienced by the signals at higher frequency (Anne, OK?).

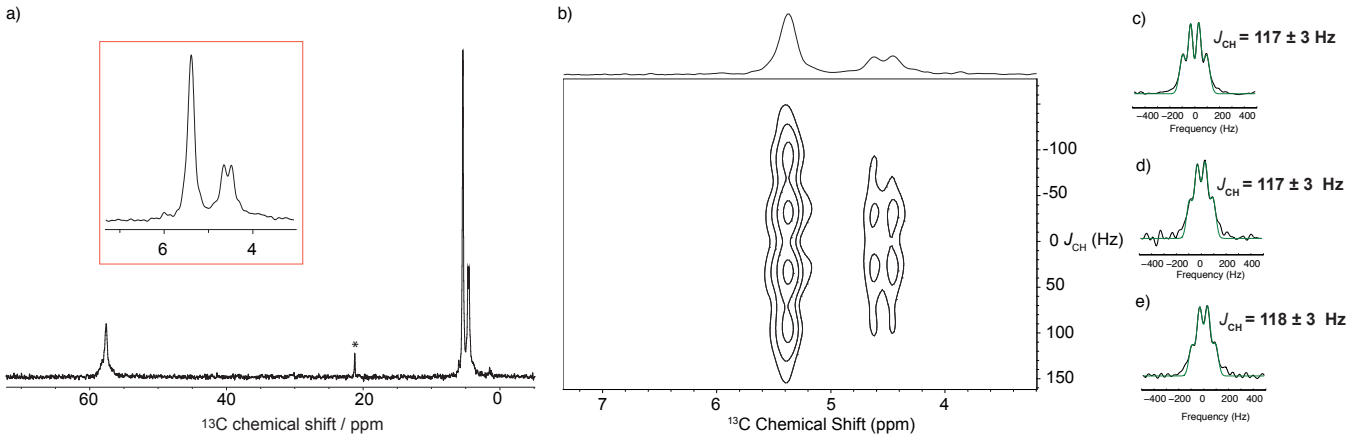

Figure 5. Solid-state NMR spectra of Lu[CH(SiMe$_3$)$_2$]$_3$; (a) ^{13}C CPMAS spectrum recorded at 10 kHz spinning speed, the red box shows an expansion of the spectrum from 3 – 7 ppm, * = toluene; (b) two-dimensional *J*-resolved spectrum of Lu[CH(SiMe$_3$)$_2$]$_3$ shown from 3 – 7 ppm; (c-e) one-dimensional traces extracted from the 2D spectrum, the values of J_{CH} for each trace are given. The black spectra are raw data, and the green spectra are the best fit of the raw data. The trace in (c) is from the signal at 5.4 ppm, the trace in (d) is from the signal at 4.7 ppm, and the trace in (e) is from the signal at 4.5 ppm.

The solid-state *J*-resolved spectrum of Lu[CH(SiMe$_3$)$_2$]$_3$, shown in Figure 5b, gives nearly identical $^1J_{CH}$ values for each of the inequivalent –SiMe$_3$ group resonances, shown in in Figures 5c – 5e as 1D traces extracted from the 2D spectrum, corroborating the solution data presented above. Similar results were obtained from the solid-state *J*-resolved spectra of Lu[CH(SiMe$_3$)$_2$]$_2$[O-2,6-*t*Bu$_2$-C$_6$H$_3$] and Lu[CH(SiMe$_3$)$_2$][O-2,6-*t*Bu$_2$-C$_6$H$_3$]$_2$ (Figure SX). These results indicate that agostic M…H–Cγ interactions are not present in solution nor in the solid state.

The Chemical Shift Anisotropy (CSA) parameters associated with the chemically inequivalent –SiMe$_3$ groups contain information about the orientational dependence of the chemical shift tensor in an external magnetic field that relates to the anisotropic distribution of electron density at the specific nucleus in question.(Textbook) The CSA is characterized by the three principal components of a second rank tensor (δ_{11}, δ_{22}, δ_{33}). The isotropic chemical shift δ_{iso} is the average of the three components, $\delta_{iso} = \frac{1}{3}(\delta_{11} + \delta_{22} + \delta_{33})$. As a result of rapid molecular tumbling, δ_{iso} is the only observable quantity in solution. The CSA is not averaged in solids and is directional, which results in a powder pattern from which the principal chemical shift components are obtained if sample spinning is slower than the magnitude of the CSA. The Herzfeld-Berger convention describes the span of the powder pattern Ω (Ω = $\delta_{11} - \delta_{33}$) and the skew κ, κ = $(\delta_{22} - \delta_{iso})/\Omega$.[22]

The ^{13}C CPMAS spectrum of Lu[CH(SiMe$_3$)$_2$]$_3$ at slow spinning speeds (1.5 kHz) shows that all of the –SiMe$_3$ resonances have very small values of the CSA that cannot be measured (due to lack of side bands). However, the ^{29}Si CPMAS of Lu[CH(SiMe$_3$)$_2$]$_3$ obtained at 1.5 kHz spinning speed results in a manifold of spinning side bands, shown in

Figure 6, from which extraction of the CSA parameters for each ^{29}Si NMR signal is possible. These values are given in Table 3. The signal at –5.3 ppm has principle components (δ_{11}, δ_{22}, δ_{33}) = (5.2, 4.1, –25.0) corresponding to a span Ω = 30.2, and the signal at –11.7 has principle components (δ_{11}, δ_{22}, δ_{33}) = (19.4, –27.1, –27.4) corresponding to a span Ω = 46.8. Both signals have similar skew (κ) values, though they differ in sign.

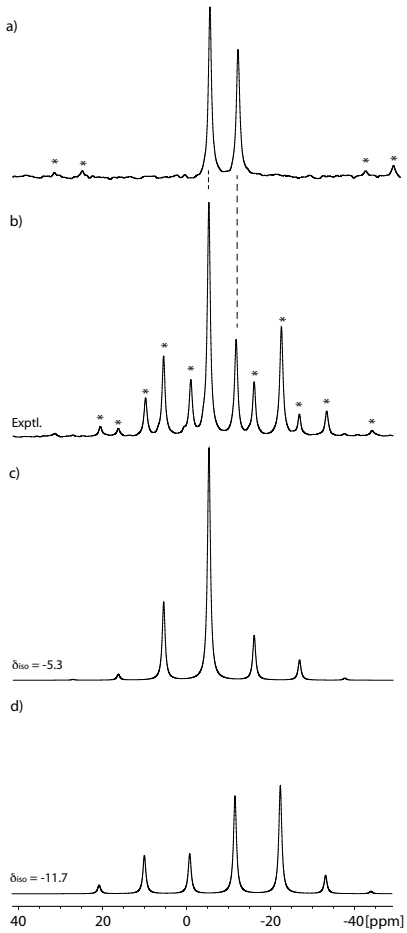

Figure 6. ^{29}Si CPMAS NMR spectrum of Lu[CH(SiMe$_3$)$_2$]$_3$; a) 5 kHz spinning rate; b) 1.5 kHz spinning rate, both spectra were recorded with a 2ms contact time; c) CSA fit for the signal at –5.3 ppm; d) CSA fit for the resonance at –11.7 ppm. The asterisks denote spinning side-bands.

Table 3. CSA parameters for the signals in the ^{29}Si CPMAS NMR spectrum of Lu[CH(SiMe$_3$)$_2$]$_3$, Lu[CH(SiMe$_3$)$_2$]$_2$[O-2,6-*t*Bu$_2$-C$_6$H$_3$], and Lu[CH(SiMe$_3$)$_2$][O-2,6-*t*Bu$_2$-C$_6$H$_3$]$_2$

	δ_{iso}	δ_{11}	δ_{22}	δ_{33}	Ω	κ
Lu[CH(SiMe$_3$)$_2$]$_3$	–5.3	5.21	4.11	–25.0	30.2	0.93
	–11.7	19.4	–27.1	–27.4	46.8	–0.98
Lu[CH(SiMe$_3$)$_2$]$_2$[O-2,6-*t*Bu-C$_6$H$_3$]	–3.1	9.8	–0.8	–21.4	31.2	0.32
	–4.2	9.0	4.4	–22.9	31.9	0.71
	–11.8	28.1	–29.1	–34.4	62.5	–0.83
	–12.7	22.3	–27.0	–33.5	55.8	–0.77
Lu[CH(SiMe$_3$)$_2$][O-2,6-*t*Bu-C$_6$H$_3$]$_2$	–4.3	15.6	–13.7	–14.8	30.3	–0.93
	–5.2	13.2	–13.6	–15.2	28.3	–0.80
	–12.8	24.4	–25.0	–37.8	62.2	–0.60
	–13.6	22.8	–28.9	–34.7	57.4	–0.80

The ^{29}Si CPMAS NMR spectrum of Lu[CH(SiMe$_3$)$_2$]$_2$[O-2,6-*t*Bu$_2$-C$_6$H$_3$] at 5 kHz spinning speed contains four signals at –3.1, –4.2, –11.8, and –12.7 ppm. The unit cell of Lu[CH(SiMe$_3$)$_2$]$_2$[O-2,6-*t*Bu$_2$-C$_6$H$_3$] contains two independent molecules, which account for the presence of four signals in the ^{29}Si CPMAS NMR spectrum. The signals at –3.1 and –4.2 ppm are approximately in a 1:1 ratio as are the resonances at –11.8 and –12.7 ppm. Extracted CSA parameters at a slower spinning rate of 1.5 kHz are given in Table 3. The signals at –3.1 and –4.2 have principle components (δ_{11}, δ_{22}, δ_{33}) = (9.8, –0.8, –21.4) and (δ_{11}, δ_{22}, δ_{33}) = (9.0, 4.4, –22.9), respectively. These values correspond to a span Ω = 31.2 and 31.9 ppm, respectively. The signals at –11.8 and –12.7 have larger Ω values of 62.5 and 55.8 ppm, respectively.

The ^{29}Si CPMAS NMR spectrum of Lu[CH(SiMe$_3$)$_2$][O-2,6-*t*Bu$_2$-C$_6$H$_3$]$_2$, which also has two independent molecules in the unit cell, contains two sets of broad signals at –4.2 and –5.2 ppm as well as –12.8 and –13.6 ppm at 5 kHz spinning rate. The CSA parameters obtained from the ^{29}Si CPMAS NMR spectrum at 1.5 kHz sample spinning are summarized in Table 3. The resonances at –4.6 and –5.2 ppm have similar Ω of 30.3 and 28.3 ppm, while the signals at –12.8 and –13.6 have a Ω of 62.2 and 57.4 ppm, respectively.

The ^{29}Si NMR parameters of Lu[CH(SiMe$_3$)$_2$]$_3$, Lu[CH(SiMe$_3$)$_2$]$_2$[O-2,6-*t*Bu-C$_6$H$_3$], and Lu[CH(SiMe$_3$)$_2$][O-2,6-*t*Bu-C$_6$H$_3$]$_2$ follow the same pattern in which one silicon atom has a large span while the other has a comparatively smaller span.

Computational Studies

The geometry of Lu[CH(SiMe$_3$)$_2$]$_3$, Lu[CH(SiMe$_3$)$_2$]$_2$[O-2,6-*t*Bu-C$_6$H$_3$], Lu[CH(SiMe$_3$)$_2$][O-2,6-*t*Bu-C$_6$H$_3$]$_2$ and Lu[O-2,6-*t*Bu-C$_6$H$_3$]$_3$ are optimized using DFT calculations. The computed geometry of the Lu-complexes are in good agreement with the solid-state structures independent of the functional used, though the Lu…Cγ distances are closest to the experimental values when small-core functionals that include dispersion are used (see the Supporting Information for details). The B3PW91-GD3BJ functional gives bond distances and angles closest to those found in their X-ray structures. Structures obtained using this functional are shown in Figure 7 and selected bond distances and angles are given in Table 4. The geometry of Lu[CH(SiMe$_3$)$_2$]$_2$[OSi(O*t*Bu)$_3$] is also calculated as a simple model for (≡SiO)Lu[CH(SiMe$_3$)$_2$]$_2$. Two geometries are located, one of which resembles the structure of Lu[CH(SiMe$_3$)$_2$]$_2$[O-2,6-*t*Bu-C$_6$H$_3$]. The other contains one short Lu…Cγ and one longer Lu…Cγ distance. The data for Lu[CH(SiMe$_3$)$_2$]$_2$[OSi(O*t*Bu)$_3$ is given in the Supplementary Information.

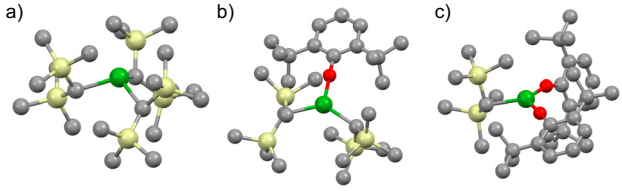

Figure 7. Calculated structures of Lu[CH(SiMe$_3$)$_2$]$_{3-x}$[O-2,6-*t*Bu-C$_6$H$_3$]$_x$ and two small molecule models of (≡SiO)Lu[CH(SiMe$_3$)$_2$]$_2$ using B3PW91-GD3BJ; (a) Lu[CH(SiMe$_3$)$_2$]$_3$; (b) Lu[CH(SiMe$_3$)$_2$]$_2$[O-2,6-*t*Bu-C$_6$H$_3$]; (c) and Lu[CH(SiMe$_3$)$_2$][O-2,6-*t*Bu-C$_6$H$_3$]$_2$.

The experimental ^{29}Si NMR parameters contain one silicon with a large Ω span and one with a smaller span. The calculated ^{29}Si NMR CSA parameters for the distal Siβ in Lu[CH(SiMe$_3$)$_2$]$_3$ has δ_{iso} = –5.2 ppm with Ω = 29.7 and κ = 0.60, while the proximal Siβ has δ_{iso} = –13.5 with Ω = 51.6 and κ = –0.48. The values of δ_{iso} and Ω are close to those obtained experimentally, even though the calculated diagonal components of the second rank tensors (δ_{11}, δ_{22}, δ_{33}) are not fully reproduced (see Table SX). In Lu[CH(SiMe$_3$)$_2$]$_2$[O-2,6-*t*Bu-C$_6$H$_3$] and Lu[CH(SiMe$_3$)$_2$][O-2,6-*t*Bu-C$_6$H$_3$]$_2$ a similar trend emerges, the Siβ proximal to Lu has a larger span value than the distal Siβ. This data further ascertains that the presence of this Lu-C interaction is associated with larger anisotropy.

Table 4. Selected of bond lengths (Å) and angles (°) of $Lu[CH(SiMe_3)_2]_x[O\text{-}2,6\text{-}t\text{Bu-}C_6H_3]_{3-x}$ (x = 1, 2, 3) and $Lu[CH(SiMe_3)_2]_2[OSi(O\text{t}Bu)_3]$ using B3PW91-GD3BJ.

	M–Cα	M…Cγ	M…Siβ[a]	Siβ–Cγ	M–Cα–Siβ	Cα–Siβ–Cγ
$Lu[CH(SiMe_3)_2]_3$	2.289	2.942[b]	3.220[b]	1.916[c] 1.885[d]	101.7 124.7	106.5
$Lu[CH(SiMe_3)_2]_2[O\text{-}2,6\text{-}t\text{Bu}_2\text{-}C_6H_3]$	2.311	2.640	3.054	1.938[c] 1.884[d]	93.8 131.9	107.4
	2.314	2.636	3.061	1.937[c] 1.884[d]	94.0 132.8	109.6
$Lu[CH(SiMe_3)_2][O\text{-}2,6\text{-}t\text{Bu}_2\text{-}C_6H_3]_2$	2.319	2.579	3.009	1.955[c] 1.884[d]	91.8 119.7	108.2

[a] – Distance from Lu to the proximal Siβ [b] – Average of three distances (specify where the data can be found) [c] – average Siβ–Cγ proximal to the lanthanide atom [d] – average of all other Siβ–Cγ d

The natural charges on the atoms in the three calculated structures are shown in Table 6. The key message is that the Cγ carbon carries a partial negative charge while the Hγ and Siβ's have partial positive charges, supporting the deduction that Lu…Cγ–Siβ is a 3c–2e interaction rather than a Lu…H–C, 3c–2e interaction. The trends in the NBO charges are remarkably constant for all atoms as C is replaced by $–O\text{-}2,6\text{-}t\text{Bu}_2\text{-}C_6H_3$, except for the positive charge on Lu, which increases slightly when the first C is replaced by $–O\text{-}2,6\text{-}t\text{Bu}_2\text{-}C_6H_3$, and somewhat more when the second C is replaced by $–O\text{-}2,6\text{-}t\text{Bu}_2\text{-}C_6H_3$. Replacing one C with $–OSi(O^tBu)_3$ results in more positive charge on Lu than replacing one C with $–O\text{-}2,6\text{-}t\text{Bu}_2\text{-}C_6H_3$ (see X). This trend is coupled with a slight increase in negative charge on the proximal Cγ atoms as shown in Table 6. These data are consistent with an increase electrophilicity of the metal sites and illustrates how the ligands modulate the relative charges in a metal-ligand bond in accordance with the Pauling's electroneutrality principle.

Table 6. Trends in NBO Charges

	$Lu[CH(SiMe_3)_2]_3$	$Lu[CH(SiMe_3)_2]_2[O\text{-}2,6\text{-}t\text{Bu-}C_6H_3]$	$Lu[CH(SiMe_3)_2][O\text{-}2,6\text{-}t\text{Bu-}C_6H_3]_2$
Lu	1.32	1.37	1.50
Cα	–1.81	–1.80	–1.80
O	–	–0.86	–0.87
Cγ[a]	–1.11	–1.14	–1.15
Cγ'[b]	–1.12	–1.12	–1.12
Siβ[a]	1.81	1.80	1.79
Siβ'[b]	1.80	1.80	1.79

[a] – proximal to Lu [b] – Average of all other values

Discussion

The experimental and computational studies outlined above were motivated by the expectation that the electrophilicity of supported organometallic compounds on silica will increase relative to the molecular precursor.(Ballard1975, WischertCS2011) The experimental studies begin with the characterization of $[(\equiv SiO)Lu[CH(SiMe_3)_2]_2]$, which contains one short intramolecular Lu…Cγ contact distance of 2.80(2) Å. The Lu–Cγ distance is longer than the direct Lu–Cα distance of 2.32(1) Å and is classified as a secondary interaction.[1, 23] In order to understand the nature of the secondary interactions in the supported compound, the structure of the surface species is compared with molecular compounds $Lu[CH(SiMe_3)_2]_3$, $Lu[CH(SiMe_3)_2]_2[O\text{-}2,6\text{-}t\text{Bu}_2\text{-}C_6H_3]$, and $Lu[CH(SiMe_3)_2][O\text{-}2,6\text{-}t\text{Bu}_2\text{-}C_6H_3]_2$ that are studied by X-ray crystallography, NMR spectroscopy and DFT calculations.

The M–Cα and M–Cγ distances in $Ln[CH(SiMe_3)_2]_3$ follow the general trend in metal radii, La[9] > Ce[8, 24] > Sm[9] > Lu (this work) (Table 7). One exception is the Sm–Cγ distance, but this distance has a large associated esd (Table 7). Contraction of the metal radius from La to Lu results in a La–Cα distance that is 0.20 Å longer than that found for Lu, and the La…Cγ distance is 0.19 Å longer than the equivalent distance in Lu. The difference between the Ln–Cα–Siβ angle in the proximal and distal $–SiMe_3$ groups of about 20° is essentially constant in the compounds listed in Table 7 as is the difference in the Cα–Siβ–Cγ angles. The bond length and angle patterns are clear; short M…Cγ–Siβ distances are associated with more acute Cα–Siβ–Cγ angles, and this distortion results in lengthening of one of the Cγ–Siβ bond distances; a similar pattern of distortions of the $La–CH(SiMe_3)_2$ group in $Cp_2^*La[CH(SiMe_3)_2]$ are found by neutron diffraction.[20]

The solid state crystal structure of $Lu[CH(SiMe_3)_2]_3$ shows that Lu lies out of the plane defined by the three carbon atoms by 0.81 Å. This distortion results in three methyl groups with short Lu…Cγ contact distances, referred to as proximal methyl groups, while the other fifteen methyl groups are distal. The Lu…Cγ distances are approximately 0.38 Å longer than the Lu–Cα distances and the former are referred to as secondary bond distances.

Table 7. Comparison of bond lengths (Å) and angles (°) for $Ln[CH(SiMe_3)_2]_3$

Ln	M– Cα	M…Cγ	M…Siβ	Siβ–Cγ	M–Cα–Siβ	Cα–Si_β–Cγ	Ref
Y	2.353(5)	2.963(6)	3.284(2)	1.925(5)[a] 1.875(1)[b]	102.1(2) 126.3(3)	106.6(3)	1
La	2.515(9)	3.121(9)	3.410(2)	1.923(1)[a] 1.866(1)[b]	102.0(4) 121.0(4)	109.7(?)	2
Ce	2.475(7)	3.068(7)	3.3884(3)	1.9251(1)[a] 1.887(1)[b]	102.8(3) 122.3(4)	108.2(4)	1
Sm	2.33(2)	2.85(3)	3.325(6)	1.946(1)[a] 1.882(1)[b,c]	107(1) 124(1)	105(1)	2
Lu	2.318(2)	2.936(2)	3.242(1)	1.908(2)[a] 1.871(4)[b]	101.9(1) 125.8(1)	106.7(1)	This work

[a] – Si_β–C_γ proximal to the lanthanide atom. [b] – average of all Si_β–C_γ distances distal to the lanthanide atom. [c] – one unusually long distal Si-Me (1.950 Å) is not included in this average distance.

This pattern in the geometry and the resulting classification of the Lu–Cα and M…Cγ distances is a general feature of the trialkyls listed in Table 7. X-Ray determined H–C bond distances and torsional angles are helpful for making the distinction between 3c–2e M…HγCγ or 3c–2e M…CγSiβ interaction when the hydrogen atoms are located and refined isotropically, but useless when the hydrogen atoms are placed in calculated positions and not refined. The Cγ–Siβ distances are in principle useful, but these distances are often statistically equal at the 3 – 5 σ confidence level. An experimental measurement that is capable of distinguishing between these two agostic models is the value of the $^1J_{CH}$ coupling constants when the fluxionality between proximal and distal Me_3Si– groups is slow. In this case $^1J_{CH}$ provides unequivocal experimental evidence about the nature of the M…Cγ interaction. In solution $Lu[CH(SiMe_3)_2]_3$ is fluxional in the ^{1}H NMR spectrum down to –100 °C, but the $–SiMe_3$ groups decoalesce by –125 °C into two chemically inequivalent, equal area resonances by –140 °C. The chemical inequivalence of the $–SiMe_3$ groups is consistent with the solid state X-ray crystal structure, but does not provide information on the nature of the interaction. The $^{13}C\{^1H\}$ chemical shifts follow a similar pattern as the ^{1}H chemical shifts as a function of temperature. The proton coupled ^{13}C NMR spectrum provides the important detail that the $^1J_{CH}$ coupling constants do not change significantly from 20 °C to –140 °C; at 20 °C $^1J_{CH}$ is 118 Hz, and at –140 °C $^1J_{CH}$ is 117 and 116 Hz in the chemically inequivalent $–SiMe_3$ groups. These results are consistent with sp^3-hybridized carbons on the proximal and distal $–SiMe_3$ groups. At –140°C the slow exchange limit, which would result in four ^{13}C resonances in a 1:1:1:3 ratio, is not reached indicating that rotation around the Si_β–C_γ bond is still rapid at this temperature. Similar trends are found for $Lu[CH(SiMe_3)_2]_2[O\text{-}2,6\text{-}t\text{Bu-}C_3H_6]$ and $Lu[CH(SiMe_3)_2][O\text{-}2,6\text{-}t\text{Bu-}C_3H_6]_2$.

The value of $^1J_{CH}$ for Cα in $Lu[CH(SiMe_3)_2]_3$, $Lu[CH(SiMe_3)_2]_2[O\text{-}2,6\text{-}t\text{Bu-}C_3H_6]$ and $Lu[CH(SiMe_3)_2][O\text{-}2,6\text{-}t\text{Bu-}C_3H_6]_2$ ranges from 91 to 96 Hz, substantially reduced relative to the $^1J_{CH}$ for the $–SiMe_3$ groups (118 Hz). At first glance this might imply an agostic Lu…HαCα interaction. However, since the lutetium is an electropositive metal atom, the s-electron density at Cα is polarized towards Lu and accordingly more p-character is present in the C–H bond, lowering $^1J_{CH}$. This application of Bent's rule is an alternative explanation for the general observation of low values of $^1J_{CH}$ in electropositive main group elements.[25]

The solid-state ^{13}C CPMAS NMR spectrum of $Lu[CH(SiMe_3)_2]_3$ at 20 °C provides definitive evidence about the nature of the Lu…Cγ interaction. The spectrum shows that the methyl resonances are resolved into three distinct resonances in the area ratio of 4:1:1 (12:3:3) (Figure 5a). This pattern indicates that one Me_3Si group contains three chemically *equivalent* methyl groups while the other contains three chemically *inequivalent* methyl groups, assuming that one resonance in the latter grouping is hidden under the former resonance. A physical process that accounts for this behavior is that rotation about one Siβ–Cα bond is free while the other is restricted. NMR relaxation measurements in the solid-state indicate that the two inequivalent $–SiMe_3$ sites have significantly shorter T_2' values (32 and 31 ms, respectively) compared to the equivalent $–SiMe_3$ sites (T_2' = 85 ms), which is consistent with a less rigid structure (Anne?) of the inequivalent $–SiMe_3$ group, due to their interaction with Lu. Further, the solid-state *J*-resolved spectrum gives equal $^1J_{CH}$ values for the three resonances, indicating a lack of asymmetry in the C-H bonds, which in turn requires that the carbon in each Si–Me group is sp^3 hybridized.

Although we were unable to measure the CSA (chemical shift anisotropy) in the ^{13}C CPMAS spectrum, which may be due to the largely unperturbed sp^3 hybridized γ-carbon, the solid-state ^{29}Si NMR spectra of $Lu[CH(SiMe_3)_2]_3$, $Lu[CH(SiMe_3)_2]_2[O\text{-}2,6\text{-}t\text{Bu-}C_3H_6]$ and $Lu[CH(SiMe_3)_2][O\text{-}2,6\text{-}t\text{Bu-}C_3H_6]_2$ contain two silicon environments in a 1:1 area ratio. In this case the CSA of both silicon atoms can be measured: one ^{29}Si NMR resonance has a narrow span (the value of Ω) indicating a more or less symmetrical silicon environment, while the other has a significantly larger Ω value indicating a more asymmetric silicon environment, which is most reasonably ascribed to the presence of the Lu…Cγ–Siβ interaction. A Neumann projection, Scheme 3, viewed down the Siβ–Cα bond is a pictorial representation of these solid-state NMR results.

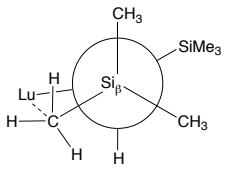

Scheme 3. Neumann projection viewed down the Siβ–Cα bond showing the Lu…Cγ–Siβ agostic interaction.

The NBO charges provide the final, and perhaps the most convincing, evidence that distinguishes between 3c–2e M…Cγ–Siβ or M…Hγ–Cγ interactions. The NBO charges on silicon in the $–SiMe_3$ groups are large and positive, and those on the hydrogen atoms are much smaller but still positive. The charge on the Cγ atoms is negative as is the charge on Cα, which is directly bonded to the positively charged Lu. Although the C atoms carry negative charges, the value on Cγ is about 40 % less than that on Cα, consistent with classification of the former as a secondary bonding interaction and the latter as a primary one. The relative signs of the NBO charges clearly indicate that the Lu–Cα and Lu…Cγ are attractive interactions while the Lu…Siβ and Lu…Hγ are repulsive.

The motivation for the studies outline in this article is to develop and use the physical properties of molecular compounds as structural models for how a solid silica support influences the physical properties of the $Lu–CH(SiMe_3)_2$ fragment in $(≡SiO)Lu[CH(SiMe_3)_2]_2$. When comparing molecular and surface species, one can see that in $(≡SiO)Lu[CH(SiMe_3)_2]_2$ the distance for the Lu…Cγ interaction lies in between those of $Lu[CH(SiMe_3)_2]_3$ and $Lu[CH(SiMe_3)_2]_2[O\text{-}2,6\text{-}t\text{Bu}_2\text{-}C_3H_6]$, which is consistent with the similar proton affinity between the two hydroxyls: 16.8(ref) for $[HO\text{-}2,6\text{-}t\text{Bu}_2\text{-}C_3H_6]$ and Y for $HOSi(OR)_3$.(Need calculated gas phase acidity, proton affinity) However, in contrast to the molecular species studied experimentally and computationally, $(≡SiO)Lu[CH(SiMe_3)_2]_2$ has an extra O-neighbor observed by EXAFS due to the presence of adjacent siloxane bridges. The presence and the strength of the Lu…Cγ interaction indicates that the electrophilicity of lutetium increases on grafting on silica and the increase is presumably the reason for the short Lu…O interaction with SiOSi group. In addition, the ^{29}Si NMR spectrum of $(≡SiO)Lu[CH(SiMe_3)_2]_2$ indicates that the $Lu–CH(SiMe_3)_2$ fragments are dynamic, which is commonly observed in mono-grafted silica-supported organometallics.[26]

Conclusions

The results outline above lead to the inescapable conclusion that the nature of the short Lu…Cγ distance in $Lu[CH(SiMe_3)_2]_x[O\text{-}2,6\text{-}t\text{Bu}_2\text{-}C_3H_6]_{3\text{-}x}$ is not due to a Lu…H–Cγ agostic interaction but to a Lu…Cγ–Siβ interaction in which the methyl group bridges the lutetium and silicon atoms.[19] The electron density in the CγSiβ σ-bond provides the electron density for the three-centered molecular orbital, as suggested by Morokuma.[18] A recent review by two of the original authors responsible for coining the adjective "agostic" states that the adjective agostic is inappropriate for such an interaction since agostic specifically refers to 3c-2e interactions involving M…H–C bonds and does not apply to all 3c-2e bonds.[1c] The classification of M…C distances as 3c-2e M…H–C agostic, rather than as a 3c-2e bridging methyl interactions brings to mind the argument about the bonding in $Me_4Al_2(μ\text{-}Me_2)_2$. The original formulation by Lougnet-Higgins [27] was that the μ-Me is a 3c-2e bridge bond analogous to his model for the bridging hydrogens in B_2H_6. An alternative model formulated the bridging methyl as a 3c-2e Al…H–C bond on the basis of X-ray diffraction data in which the hydrogen atoms were neither located nor refined.[28] Cotton pointed out that the reformulation was "unjustified, incorrect and misleading".[29] A low temperature X-ray data set was obtained, in which the hydrogen atoms were located and refined,[30] is consistent with the Lougnet-Higgins model. An extension of the model by Morokuma [18, 31] was used to explain the bonding between Ti and the γ-methyl group in $Cp_2Ti–C(SiMe_3)=C(Me)(Ph)^+$ and here between Lu and a γ-methyl group in $Lu[CH(SiMe_3)_2]_3$ and related compounds (Table 7). The Lu…Cγ distance in $(≡SiO)Lu[CH(SiMe_3)_2]_2$ lies in between that found in $Lu[CH(SiMe_3)_2]_3$ and in $Lu[CH(SiMe_3)_2]_2[O\text{-}2,6\text{-}t\text{Bu}\text{-}C_6H_3]$. The Lu–Cγ distance gets shorter as the number of oxygen-containing ligands increase, and is modulated by the siloxane bridge in the silica-supported compound. This interaction is associated with the increase of positive charge on Lu and therefore with the increase in electrophilicity at the metal sites. This interaction is particularly favorable in the compounds described in this article since Lu is three-coordinate and coordinatively unsaturated. The strength of the Lu–Cγ interaction also demonstrates the effect of introducing a surface siloxy ligand in the coordination sphere of a low coordinate metal site, and shows how silica modulates the electrophilicity of surface sites by making them better Lewis acids. The use of solid-state NMR spectroscopy outline above illustrates the power of this technique to provide unprecedented details about structure and bonding in molecular and surface species. Future studies will develop this theme.

ASSOCIATED CONTENT

Supporting Information

The Supporting Information is available free of charge on the ACS Publications website.

Solution NMR, additional solid-state NMR spectra, crystallographic tables, computational details. (PDF)

Crystallographic data (CIF)

AUTHOR INFORMATION

Corresponding Author

* ccoperet@ethz.ch; raandersen@lbl.gov

Funding Sources

Any funds used to support the research of the manuscript should be placed here (per journal style).

ACKNOWLEDGMENT

CC thanks the Miller Institute for a Visiting Professor position at UC Berkeley, during which this manuscript was finalized. Portions of this work were performed at Lawrence Berkeley National Laboratory under Contract No. DE-AC02-05CH11231 and at the Stanford Synchrotron Radiation Lightsource (SSRL). Use of the Stanford Synchrotron Radiation Lightsource, SLAC National Accelerator Laboratory, is supported by the U.S. Department of Energy, Office of Science, Office of Basic Energy Sciences under Contract No. DE-AC02-76SF00515.

REFERENCES

TOC

Si_β-C_γ polarization modulated by Electrophilic Metal Sites

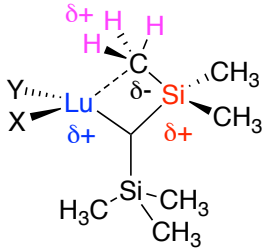

Highlighted by
^{13}C and ^{29}Si solid-state NMR
DFT Calculations
X-ray Adsorption and Diffraction

δ+ at Lu: X = Y = Alkyl < X = Alkyl, Y= OR < Y = X = OR

Need to change TOC to discuss silica vs. the rest

---

[1] aM. Brookhart, M. L. H. Green, *Journal of Organometallic Chemistry* **1983**, *250*, 395-408; bM. Brookhart, M. L. H. Green, L. L. Wong, *Prog. Inorg. Chem.* **1988**, *36*, 1-124; cM. Brookhart, M. L. H. Green, G. Parkin, *Proceedings of the National Academy of Sciences of the United States of America* **2007**, *104*, 6908-6914.

[2] aG. W. Coates, *Chemical Reviews* **2000**, *100*, 1223-1252; bR. H. Grubbs, G. W. Coates, *Accounts of Chemical Research* **1996**, *29*, 85-93; cH. H. Brintzinger, D. Fischer, R. Mülhaupt, B. Rieger, R. M. Waymouth, *Angewandte Chemie International Edition in English* **1995**, *34*, 1143-1170; dS. D. Ittel, L. K. Johnson, M. Brookhart, *Chemical Reviews* **2000**, *100*, 1169-1204.

[3] aJ. H. Oskam, R. R. Schrock, *Journal of the American Chemical Society* **1993**, *115*, 11831-11845; bH. Jeong, J. M. John, R. R. Schrock, A. H. Hoveyda, *Journal of the American Chemical Society* **2015**, *137*, 2239-2242; cH. Jeong, J. M. John, R. R. Schrock, *Organometallics* **2015**; dR. R. Schrock, W. E. Crowe, G. C. Bazan, M. DiMare, M. B. O'Regan, M. H. Schofield, *Organometallics* **1991**, *10*, 1832-1843; eR. R. Schrock, *Chemical Reviews* **2009**, *109*, 3211-3226; fJ. H. Oskam, R. R. Schrock, *Journal of the American Chemical Society* **1992**, *114*, 7588-7590; gM. M. Flook, J. B√∂rner, S. M. Kilyanek, L. C. H. Gerber, R. R. Schrock, *Organometallics* **2012**, *31*, 6231-6243.

[4] aJ. F. Hartwig, *Organotransition Metal Chemistry: From Bonding to Catalysis*, University Science Books, **2010**; bR. N. Perutz, S. Sabo-Etienne, *Angewandte Chemie International Edition* **2007**, *46*, 2578-2592.

[5] aZ. Dawoodi, M. L. H. Green, V. S. B. Mtetwa, K. Prout, A. J. Schultz, J. M. Williams, T. F. Koetzle, *Journal of the Chemical Society, Dalton Transactions* **1986**, 1629-1637; bZ. Dawoodi, M. L. H. Green, V. S. B. Mtetwa, K. Prout, *Journal of the Chemical Society, Chemical Communications* **1982**, 802-803.

[6] aX. Solans-Monfort, E. Clot, C. Cop√©ret, O. Eisenstein, *Organometallics* **2005**, *24*, 1586-1597; bA. Poater, X. Solans-Monfort, E. Clot, C. Coperet, O. Eisenstein, *Dalton Transactions* **2006**, 3077-3087.

[7] M. Brookhart, M. L. H. Green, R. B. A. Pardy, *Journal of the Chemical Society, Chemical Communications* **1983**, 691-693.

[8] A. G. Avent, C. F. Caro, P. B. Hitchcock, M. F. Lappert, Z. Li, X.-H. Wei, *Dalton Transactions* **2004**, 1567-1577.

[9] P. B. Hitchcock, M. F. Lappert, R. G. Smith, R. A. Bartlett, P. P. Power, *Journal of the Chemical Society, Chemical Communications* **1988**, 1007-1009.

[10] aG. Jeske, H. Lauke, H. Mauermann, P. N. Swepston, H. Schumann, T. J. Marks, *Journal of the American Chemical Society* **1985**, *107*, 8091-8103; bD. Stern, M. Sabat, T. J. Marks, *Journal of the American Chemical Society* **1990**, *112*, 9558-9575; cM. A. Giardello, V. P. Conticello, L. Brard, M. Sabat, A. L. Rheingold, C. L. Stern, T. J. Marks, *Journal of the American Chemical Society* **1994**, *116*, 10212-10240; dC. J. Schaverien, A. G. Orpen, *Inorganic Chemistry* **1991**, *30*, 4968-4978; eJ. Cheng, J. Takats, M. J. Ferguson, R. McDonald, *Journal of the American Chemical Society* **2008**, *130*, 1544-1545; fS. Tian, V. M. Arredondo, C. L. Stern, T. J. Marks, *Organometallics* **1999**, *18*, 2568-2570; gH. J. Heeres, J. Renkema, M. Booij, A. Meetsma, J. H. Teuben, *Organometallics* **1988**, *7*, 2495-2502; hH. Schumann, E. C. E. Rosenthal, G. Kociok-K√∂hn, G. A. Molander, J. r. Winterfeld, *Journal of Organometallic Chemistry* **1995**, *496*, 233-240; iC. J. Schaverien, G. J. Nesbitt, *Journal of the Chemical Society, Dalton Transactions* **1992**, 157-167.

[11] aC. Copéret, M. Chabanas, R. Petroff Saint-Arroman, J.-M. Basset, *Angewandte Chemie International Edition* **2003**, *42*, 156-181; bF. Rascon, R. Wischert, C. Coperet, *Chemical Science* **2011**, *2*, 1449-1456; cD. Gajan, C. Coperet, *New Journal of Chemistry* **2011**, *35*, 2403-2408; dM. Conley, C. Copéret, *Top. Catal.* **2014**, *57*, 843-851.

[12] D. C. Bradley, J. S. Ghotra, F. A. Hart, *J. Chem. Soc.* **1973**, 1021.

[13] M. F. Lappert, A. Singh, R. G. Smith, H. A. Stecher, A. Sen, in *Inorg. Synth.*, John Wiley & Sons, Inc., **2007**, pp. 164-168.

[14] E. Le Roux, M. Chabanas, A. Baudouin, A. de Mallmann, C. Copéret, E. A. Quadrelli, J. Thivolle-Cazat, J.-M. Basset, W. Lukens, A. Lesage, L. Emsley, G. J. Sunley, *J. Am. Chem. Soc.* **2004**, *126*, 13391-13399.

[15] aA. H. Cowleya, R. A. Kemp, *Synth. React. Inorg. Met.-Org. Chem.* **1981**, *11*, 591-595; bP. J. Davidson, D. H. Harris, M. F. Lappert, *Journal of the Chemical Society, Dalton Transactions* **1976**, 2268-2274.

[16] aG. R. Giesbrecht, J. C. Gordon, D. L. Clark, B. L. Scott, *Inorg. Chem.* **2004**, *43*, 1065-1070; bM. Konkol, T. P. Spaniol, M. Kondracka, J. Okuda, *Dalton Trans.* **2007**, 4095-4102; cA. Fischbach, E. Herdtweek, R. Anwander, G. Eickerling, W. Scherer, *Organometallics* **2003**, *22*, 499-509.

[17] W. Scherer, G. S. McGrady, *Angewandte Chemie International Edition* **2004**, *43*, 1782-1806.

[18] N. Koga, K. Morokuma, *Journal of the American Chemical Society* **1988**, *110*, 108-112.

[19] aT. D. Tilley, R. A. Andersen, A. Zalkin, *Journal of the American Chemical Society* **1982**, *104*, 3725-3727; bS. S. Rozenel, R. A. Andersen, *Inorganica Chimica Acta* **2014**, *422*, 202-205.

[20] W. T. Klooster, L. Brammer, C. J. Schaverien, P. H. M. Budzelaar, *Journal of the American Chemical Society* **1999**, *121*, 1381-1382.

[21] E. J. Stoebenau Iii, R. F. Jordan, *Journal of Organometallic Chemistry* **2006**, *691*, 4956-4962.

[22] J. Herzfeld, A. E. Berger, *J. Chem. Phys.* **1980**, *73*, 6021-6030.

[23] E. Clot, O. Eisenstein, *Principles and Applications of Density in Inorganic Chemistry Ii* **2004**, *113*, 1-36.

[24] aH. J. Heeres, J. H. Teuben, R. D. Rogers, *Journal of Organometallic Chemistry* **1989**, *364*, 87-96; bM. Booij, N. H. Kiers, H. J. Heeres, J. H. Teuben, *Journal of Organometallic Chemistry* **1989**, *364*, 79-86.

[25] B. E. Mann, B. F. Taylor, *13C NMR data for organometallic compounds*, Academic Press, **1981**.

[26] F. Blanc, J.-M. Basset, C. Copéret, A. Sinha, Z. J. Tonzetich, R. R. Schrock, X. Solans-Monfort, E. Clot, O. Eisenstein, A. Lesage, L. Emsley, *Journal of the American Chemical Society* **2008**, *130*, 5886-5900.

[27] H. C. Longuet-Higgins, *Journal of the Chemical Society (Resumed)* **1946**, 139-143.

[28] S. K. Byram, J. K. Fawcett, S. C. Nyburg, R. J. O'Brien, *Journal of the Chemical Society D: Chemical Communications* **1970**, 16-17.

[29] F. A. Cotton, *Inorganic Chemistry* **1970**, *9*, 2804-2804.

[30] J. C. Huffman, W. E. Streib, *Journal of the Chemical Society D: Chemical Communications* **1971**, 911-912.

[31] aM. P. Mitoraj, A. Michalak, T. Ziegler, *Organometallics* **2009**, *28*, 3727-3733; bL. Perrin, L. Maron, O. Eisenstein, M. F. Lappert, *New Journal of Chemistry* **2003**, *27*, 121-127.